Rotational excitation of mono- and doubly-deuterated water by hydrogen molecules

A. Faure, Laurent Wiesenfeld, Yohann Scribano, C. Ceccarelli

Monthly Notices
of the
ROYAL ASTRONOMICAL SOCIETY

Mon. Not. R. Astron. Soc. **420,** 699–704 (2012) doi:10.1111/j.1365-2966.2011.20081.x

Rotational excitation of mono- and doubly-deuterated water by hydrogen molecules

A. Faure,[1⋆] L. Wiesenfeld,[1] Y. Scribano[2] and C. Ceccarelli[1]

[1] *UJF-Grenoble 1/CNRS-INSU, Institut de Planétologie et d'Astrophysique de Grenoble (IPAG) UMR 5274, Grenoble F-38041, France*
[2] *Laboratoire Interdisciplinaire Carnot de Bourgogne-UMR 5209, CNRS-Université de Bourgogne, 9 Av. Alain Savary, B.P. 47870, F-21078 Dijon Cedex, France*

Accepted 2011 October 26. Received 2011 October 25; in original form 2011 September 1

ABSTRACT

Rate coefficients for rotational transitions in HDO and D_2O induced by H_2 collisions below 300 K are presented. Calculations have been performed at the close-coupling and coupled-states levels with the deuterated variants of the H_2O–H_2 interaction potential of Valiron et al. The HDO–H_2 and D_2O–H_2 rate coefficients are compared to the corresponding rate coefficients for HDO–He and H_2O–H_2, respectively. Significant differences are observed. In particular the new HDO rate coefficients are found to be significantly larger (by up to three orders of magnitude) than the corresponding HDO–He rate coefficients. The impact of the new HDO rate coefficients is examined with the help of non-LTE radiative transfer calculations. A number of potential HDO maser lines are finally identified, in particular the 80.6 GHz ($1_{1,0}$–$1_{1,1}$) transition.

Key words: molecular data – molecular processes – stars: formation – ISM: molecules.

1 INTRODUCTION

Despite the low cosmic deuterium abundance, D/H $\sim 10^{-5}$, a spectacular deuterium enrichment of various interstellar molecules is observed in star-forming regions (Ceccarelli et al. 2007, and references therein). Among these molecules, the deuterated isotopologues of water, HDO and D_2O are of special importance because they can help to understand the origin of water in the interstellar medium and its possible link with the D/H ratios observed in comets and in the Earth's oceans ($\sim 10^{-4}$) (Hartogh et al. 2011). While interstellar HDO was detected a few years after the discovery of H_2O in the interstellar medium (Turner et al. 1975), D_2O has been identified only recently towards the protostar IRAS 16293−2422 (Butner et al. 2007). Investigation of the abundance of water and its isotopologues in space is one of the main targets of the heterodyne instrument for the infrared (HIFI) aboard *Herschel Space Observatory*, which was launched in 2009 May. Recent HIFI detections towards star-forming regions include HDO (Ceccarelli et al. 2010a; Comito et al. 2010; Coutens et al. 2011) and D_2O (Vastel et al. 2010) as well as the first (tentative) identification of $HD^{18}O$ (Bergin et al. 2010).

As the densities in star-forming regions are low ($n \lesssim 10^8$ cm^{-3}), the molecular populations are generally not at local thermodynamical equilibrium (LTE) but rather they are determined by a competition between radiative and collisional processes. The computation of molecular abundances therefore relies on radiative transfer modelling which involves the knowledge of rate coefficients for collisional (de-)excitation. As it is extremely difficult to determine these coefficients experimentally, radiative transfer models can only rely on theoretical predictions. Until recently, the only available collisional rate coefficients for deuterated water were those of Green for HDO with He (Green 1989) and those of Faure et al. for electron-impact excitation of HDO and D_2O (Faure, Gorfinkiel & Tennyson 2004). However, in regions where HDO and D_2O are abundant, the main colliding partner is H_2.

Here we report the computation of collisional rate coefficients for the rotational (de-)excitation of HDO and D_2O by H_2 molecules. Preliminary calculations have been reported by Scribano, Faure & Wiesenfeld (2010) for D_2O–H_2 and by Wiesenfeld, Scribano & Faure (2011) for HDO–H_2. These authors have presented detailed comparisons between the three water–hydrogen isotopologues H_2O–H_2, HDO–H_2 and D_2O–H_2. Significant differences were observed and they were attributed to symmetry, kinematics and intramolecular geometry effects. Moreover, in the case of HDO, rate coefficients with H_2 were found significantly larger than the HDO–He rate coefficients of Green (1989) which are currently employed in astronomical models. The aim of this paper is (i) to present the full set of collisional rate coefficients for HDO and D_2O and (ii) to investigate the impact of these new rate coefficients on non-LTE radiative transfer calculations. A brief description of the scattering calculations is presented in Section 2 along with a presentation of the rate coefficients. The general impact of the new HDO rate coefficients on radiative transfer computations is presented in Section 3. The specific case of maser transitions is discussed in Section 4. Conclusions are drawn in Section 5.

⋆E-mail: afaure@obs.ujf-grenoble.fr

2 SCATTERING CALCULATIONS

All scattering calculations were performed using the full nine-dimensional potential energy surface (PES) for H_2O–H_2 (Faure et al. 2005; Valiron et al. 2008). This *ab initio* PES was obtained by combining standard coupled-cluster [CCSD(T)] calculations with explicitly correlated CCSD(T)–R12 calculations. Full details can be found in Valiron et al. (2008). This PES is independent of nuclear masses and can be employed for any water–hydrogen isotopologue. Its high accuracy has been spectacularly confirmed very recently by a number of comparisons between theory and experiment including inelastic total and differential cross-sections (Yang et al. 2010, 2011), pressure broadening cross-sections (Wiesenfeld & Faure 2010), elastic integral cross-sections (Belpassi et al. 2010) and the spectrum of the van der Waals complex (van der Avoird & Nesbitt 2011; van der Avoird et al. 2011; Wang & Carrington 2011).

The HDO–H_2 and D_2O–H_2 rigid-rotor PESs were obtained from the full flexible H_2O–H_2 potential, but in the principal inertia axes of the water isotopologues and fixing the internal coordinates at their vibrationally averaged values. Full details can be found in Scribano, Faure & Wiesenfeld (2010) and Wiesenfeld, Scribano & Faure (2011).

The quantum theory for scattering of an asymmetric top with a linear molecule can be found in Phillips, Maluendes & Green (1995). The rotational energy levels of the water isotopologues are labelled by three numbers: the angular momentum j_1 and the pseudo-quantum numbers k_a and k_c, which correspond to the projection of j_1 along the principal inertia a- and c-axes. The rotational levels of the projectile H_2 are labelled by the angular momentum j_2. In the present work, calculations were performed using the OpenMP version of the scattering code MOLSCAT.[1] All calculations for D_2O were performed at the close-coupling (CC) level while for HDO the coupled-states (CS) approximation, which approximates certain Coriolis-coupling terms, was employed at the highest energies (see below). In the case of D_2O, the initial H_2 was restricted to its lowest para state ($j_2 = 0$) because the fraction of ortho-H_2 ($j_2 = 1$) is expected to be negligible in the coldest interstellar regions ($T < 30$ K) where D_2O is abundant (Troscompt et al. 2009; Vastel et al. 2010). In contrast, HDO is observed both in cold and warm ($T > 100$ K) environments (e.g. Coutens et al., in preparation). In these latter cases, the fractions of ortho-H_2 in $j_2 = 1$ and para-H_2 in $j_2 = 2$ are expected to be significant. In the case of HDO, the initial H_2 was therefore taken in its lowest para ($j_2 = 0, 2$) and ortho ($j_2 = 1$) levels.

All calculations included several energetically inaccessible (closed) channels to ensure that cross-sections were converged to within 5 per cent for all transitions involving levels with energies below $\sim$100 cm^{-1}. For higher levels in HDO, cross-sections were converged to within 20 per cent. The lowest 12 D_2O levels were considered, i.e. up to the para level $3_{1,2}$ at 89.97 cm^{-1} and up to the ortho level $3_{1,3}$ at 74.51 cm^{-1}. We note that since the ortho and para levels of D_2O do not interconvert in inelastic collisions, they were treated separately. The basis set for D_2O incorporated all target states with $j_1 \leq 6$. In the case of HDO, the lowest 30 levels were considered, i.e. up to the level $6_{1,6}$ at 308.62 cm^{-1}. The basis set for HDO incorporated all target states up to $j_1 \leq 9$ (limited to an energy of 1100 cm^{-1}) for CC calculations and up to $j_1 \leq 11$ (limited to an energy of 1710 cm^{-1}) for CS calculations. The inclusion of the $j_2 = 2$ level of H_2, which opens at 365 cm^{-1}, was found to be necessary at all collision energies for both isotopologues. In contrast, the level $j_2 = 3$, which opens at 730 cm^{-1}, was found to have a minor influence ($\leq$10 per cent) and was therefore neglected.

CC calculations for D_2O were performed at total energies $E_{\rm tot} \leq 600$ cm^{-1}. In the case of HDO, CC calculations were performed at $E_{\rm tot} \leq 338$ cm^{-1} for para-H_2 ($j_2 = 0, 2$) and $E_{\rm tot} \leq 551$ cm^{-1} for ortho-H_2 ($j_2 = 1$). At higher energies, the CC method becomes prohibitively expensive and the CS approximation was adopted up to $E_{\rm tot} = 15000$ cm^{-1}. The CS cross-sections were however scaled to match the CC results at the highest value of the overlapping energy range, as in Wiesenfeld et al. (2011). We also note that a few number of transitions have zero cross-sections within the CS approximation. For these, the CC results were simply extrapolated by a constant. Full details can be found in Scribano et al. (2010) and Wiesenfeld et al. (2011). Rate coefficients were obtained by integrating the cross-sections over Maxwell–Boltzmann distributions of relative velocities. For HDO colliding with para-H_2, the rate coefficients were also summed at each temperature over the final levels of H_2 ($j_2' = 0, 2$) and averaged over the initial levels of H_2 ($j_2 = 0, 2$), assuming these latter have a thermal distribution. In practice, the contribution of the initial level $j_2 = 2$ was found to be significant when the temperature exceeds about 100 K.

The rate coefficients for D_2O–H_2 and HDO–H_2 were obtained in the temperature ranges 5–100 and 5–300 K, respectively. The typical temperature dependences of the rate coefficients, the discussion of propensity rules and the comparison between para-H_2 ($j_2 = 0$) and ortho-H_2 ($j_2 = 1$) can be found in Wiesenfeld et al. (2011). We note in particular that in the case of HDO, the shift of the centre of mass is crucial because it breaks the C_{2v} symmetry and induces additional (a-type) transitions with significant rate coefficients (Wiesenfeld et al. 2011). An overall presentation of the D_2O rate coefficients at 20 K is given in Fig. 1. In this plot, the

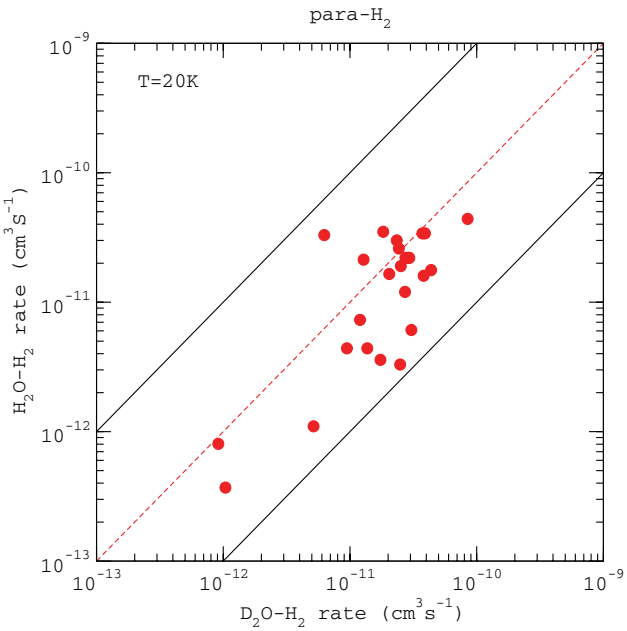

Figure 1. Comparison between the rate coefficients for D_2O and H_2O colliding with para-H_2 ($j_2 = 0$). De-excitation transition rate coefficients are reported for the lowest 12 rotational levels at 20 K. The horizontal axis represents the present D_2O rate coefficients (in units of cm^3 s^{-1}) and the vertical axis represents the corresponding H_2O rate coefficients from Dubernet et al. The two solid lines delimit the region where the rate coefficients differ by less than a factor of 10. See text for details.

[1] Repository at http://ipag.osug.fr/~afaure/molscat/index.html.

D_2O rate coefficients are plotted versus the corresponding H_2O rate coefficients for de-excitation transitions involving the lowest 12 rotational levels. The H_2O rate coefficients with para-H_2 ($j_2 = 0$) were taken from Dubernet et al. (2006, 2009). It should be noted that these H_2O rate coefficients were obtained at the same level of accuracy as the present calculations using the H_2O–H_2 PES of Faure et al. (2005). We also note that the ortho and para symmetries are reversed in D_2O with respect to H_2O so that transitions in ortho-D_2O are compared to the corresponding ones in para-H_2O and vice versa. It can be observed that D_2O and H_2O rate coefficients generally agree within a factor of 2–3, but differences as large as a factor of ∼8 exist. These differences are caused by the isotopic substitution only and they were attributed by Scribano et al. (2010) to both kinematics (i.e. mass and velocities) and intramolecular geometry effects. We conclude that H/D isotopic substitution has a significant effect (for molecules of the size of H_2O) and that the rate coefficients for the main isotopologue provide only estimates for the deuterated species, at the order-of-magnitude level.

An overall presentation of the HDO rate coefficients at 50 and 100 K is given in Fig. 2. In this plot, the new HDO rate coefficients are plotted versus the HDO–He rate coefficients of Green (1989) for all de-excitation transitions involving the lowest 30 levels. It should be noted that the HDO–He rate coefficients were scaled by the factor of 1.35 to account for the ratio of the reduced masses between HDO–H_2 and HDO–He. A large dispersion of the rate coefficients is observed and we can note that a significant fraction of the (scaled) He rate coefficients differ from the H_2 rate coefficients by more than a factor of 10. In fact, most of the ortho-H_2 rate coefficients exceed the corresponding He rate coefficients by more than a factor of 10 and some of them by up to three orders of magnitude. We also observe that, on average, rate coefficients with ortho-H_2 ($j_2 = 1$) are a factor of ∼5 larger than the corresponding rate coefficients for the thermalized para-H_2 ($j_2 = 0, 2$). We conclude that He is not a good substitute for H_2 in the case of HDO, as already observed for H_2O (Faure et al. 2007; Dubernet et al. 2009). It should be noted, however, that the large differences observed here between He and H_2 partly reflect differences in the accuracy of the corresponding PES. Indeed, in the case of H_2O–He, Yang & Stancil (2007) have found that the state-to-state rate coefficients based on modern accurate PES are larger than the corresponding rate coefficients obtained from the PES of Palma et al. (1988), i.e. the one employed by Green (1989) for HDO–He, by up to a factor of 2 at 50 K. In any case, a significant impact of the new HDO rate coefficients is thus expected in the determination of interstellar HDO abundances, as examined below.

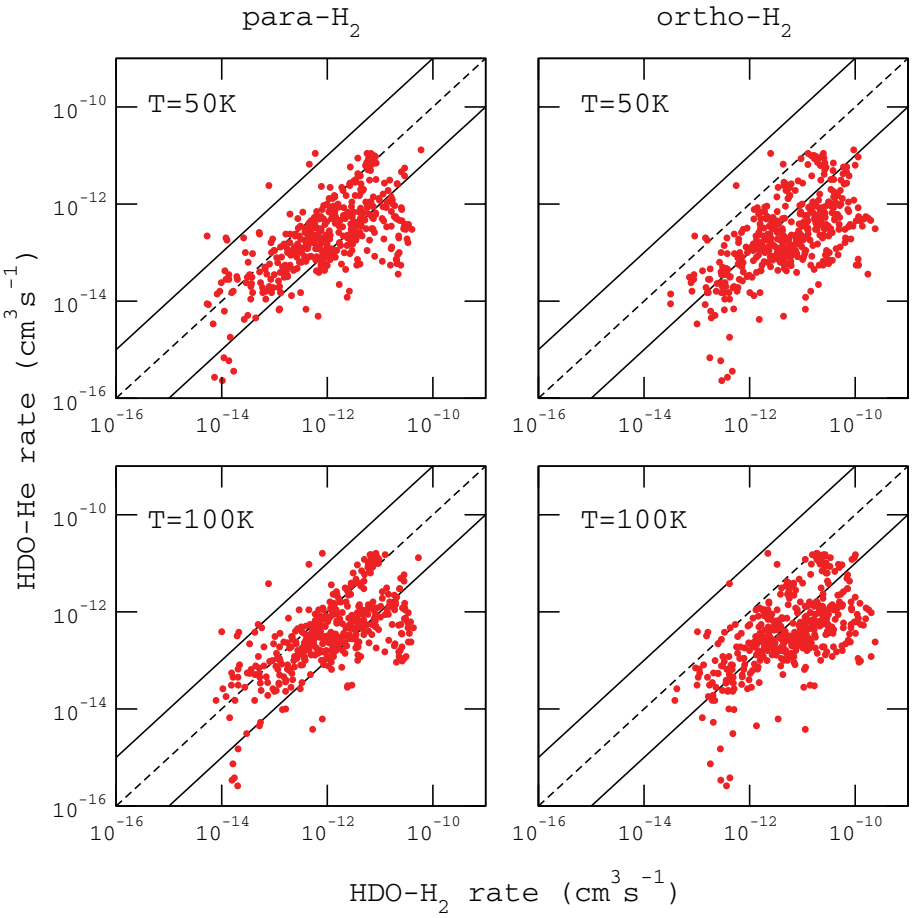

Figure 2. Comparison between the rate coefficients for HDO–H_2 and HDO–He. De-excitation transition rate coefficients are reported for the lowest 30 rotational levels at 50 and 100 K. The horizontal axis represents the present HDO–H_2 rate coefficients (in units of $cm^3\ s^{-1}$) and the vertical axis represents the corresponding (scaled) HDO–He rate coefficients from Green (1989). Left- and right-hand panels correspond to thermalized para-H_2 ($j_2 = 0, 2$) and ortho-H_2 ($j_2 = 1$), respectively. The two solid lines delimit the region where the rate coefficients differ by less than a factor of 10. See text for details.

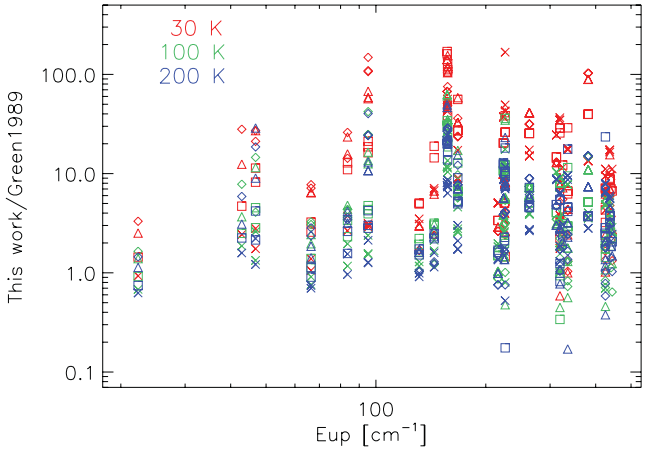

Figure 3. Ratio of the brightness temperature T_B values of different transitions calculated with the present rate coefficients with respect to the Green (1989) rate coefficients, as a function of the upper level energy of the transition. Different colours refer to different temperatures: 30 K (red), 100 K (green) and 200 K (blue). Different symbols refer to different densities: 10^5 cm^{-3} (diamonds), 10^6 cm^{-3} (triangles), 10^7 cm^{-3} (squares) and 10^8 cm^{-3} (crosses). In these computations, a HDO column density of 10^{14} cm^{-2} (km s^{-1})$^{-1}$ was adopted.

We note finally that the full sets of HDO and D_2O rate coefficients are made available in the LAMDA data base[2] as well as at the Centre de données astronomiques de Strasbourg (CDS).[3] As explained above, the rate coefficients for HDO colliding with para-H_2 are summed and averaged assuming a thermal distribution of $j_2 = 0, 2$. However, for applications where the H_2 rotational populations are not thermalized, the j_2-resolved rate coefficients can be obtained upon request to the authors.

3 IMPACT OF THE NEW HDO COLLISION RATE COEFFICIENTS

In order to estimate the impact of the new rate coefficients on the HDO abundance derived from observations, we have performed non-LTE radiative transfer calculations with the two sets of rate coefficients, the old ones from Green (1989) and the new ones from this work. The large velocity gradient (LVG) approximation was employed with a code adapted from the one described in Ceccarelli et al. (2003). It refers to a semi-infinite isodense and isothermal slab in plane-parallel geometry. The first 30 levels of HDO were included. The ortho-to-para ratio of H_2 is taken at its thermodynamic equilibrium value for each temperature. As a background radiation field, we included the 2.7 K cosmic microwave background only. Fig. 3 gives an overview of the results for all lines in the 0–2000 GHz frequency range and with an upper level energy lower than 150 K. Specifically, we plot the ratio between the brightness temperature T_B values calculated with the new rate coefficients and those calculated with the Green (1989) rate coefficients, for different densities and temperatures, in the optically thin case. Fig. 3 makes it very clear that this ratio is between 3 and 30 for most of the quoted transitions and that it can be as high as 100 for a few of them, in the range of temperature (30–200 K), densities (10^5–10^8 cm^{-3}) and HDO column density (10^{14}–10^{17} cm^{-2}) explored here. We conclude that in the optically thin case, the inaccuracies in excitation

[2] http://www.strw.leidenuniv.nl/~moldata/ (Schöier et al. 2005)
[3] http://cdsweb.u-strasbg.fr

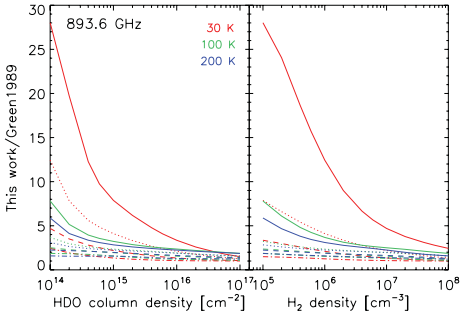

Figure 4. Transition $1_{1,1}$–$0_{0,0}$ at frequency 893.6 GHz. Ratio of the T_B values calculated with the present rate coefficients with respect to the Green (1989) rate coefficients as a function of the HDO column density (left-hand panel) and H_2 density (right-hand panel). Different colours refer to different temperatures: 30 K (red), 100 K (green) and 200 K (blue). In the left-hand panel, different lines refer to different H_2 densities: 10^5 cm^{-3} (solid line), 10^6 cm^{-3} (dotted line), 10^7 cm^{-3} (dashed line) and 10^8 cm^{-3} (dash–dotted line). In the right-hand panel, different lines refer to different HDO column densities: 10^4 cm^{-2} (solid line), 10^{15} cm^{-2} (dotted line), 10^{16} cm^{-2} (dashed line) and 10^{17} cm^{-2} (dash–dotted line).

rate coefficients are quasi-linearly propagated within the radiative transfer equations. This implies a possible overestimation of the HDO abundance (and therefore of the D/H ratio of water) in the emitting region by the same value, depending on the used line.

Fig. 3 also shows that the largest ratios are obtained at the lowest H_2 densities and temperatures. This is expected since the farther from the LTE, the larger the importance of the employed excitation rate coefficients on the level population. However, this is not strictly true in all situations. Some specific cases of used HDO lines are reported in Figs 4–6, in order to show how exactly the ratio depends on the density and temperature of the gas as well as on the HDO column density (namely the line's optical depth). Fig. 4 shows the specific case of the HDO line $1_{1,1}$–$0_{0,0}$ at 893 GHz. The impact of the new rate coefficients on this line is large at low temperatures and low densities, as the ratio can be a factor of almost 30. The largest difference occurs at the lowest HDO column density (left-hand panel), where the line optical depths do not influence the levels population. At large enough HDO column densities, the ratio tends to be less than 2. Figs 5 and 6 report two cases where the impact of the new collisional coefficients is particularly large, and the difference between the present and old collisional coefficients leads to factors of larger than 100. In the case of the 241-GHz line, often observed, the largest difference between the two sets of rate coefficients is not necessarily obtained at the

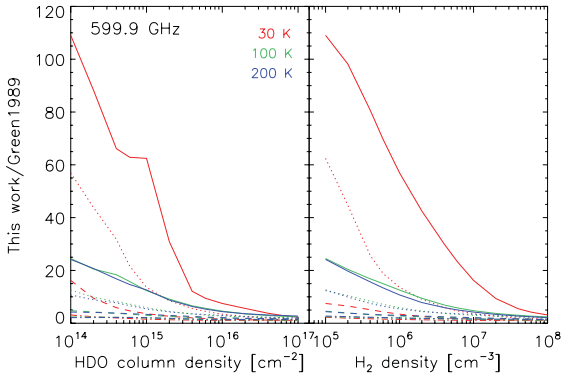

Figure 5. Same as Fig. 4, but for the transition $2_{1,1}$–$2_{0,2}$ at frequency 599.9 GHz.

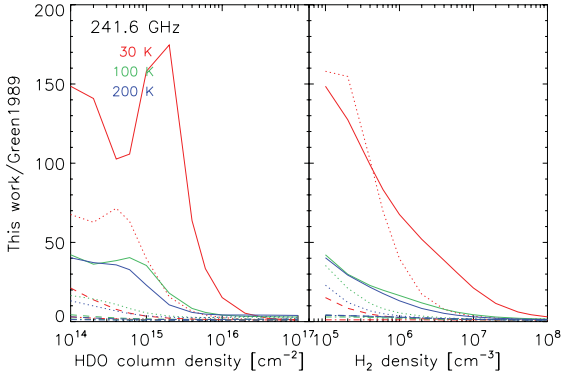

Figure 6. Same as Fig. 4, but for the transition $2_{1,1}$–$2_{1,2}$ at frequency 241.6 GHz.

lowest column densities (left-hand panel). Indeed, the maximum difference is found to peak at $\sim 2 \times 10^{15}$ cm^{-2}. It should be noted that the oscillation of the plotted ratio in the range 10^{14}–10^{15} cm^{-2} is not unphysical: the brightness temperatures were checked and they show a perfectly smooth dependence with respect to the column density. This oscillation simply reflects the great sensitivity of radiative transfer equations to the excitation rate coefficients in this range of column density. We finally note that for the majority of the lines, the largest difference between the two sets of rate coefficients peaks at densities around 10^5 cm^{-3}, which is consistent with the typical value of the critical density, $n_{\rm cr} \sim 10^7$ cm^{-3}.

4 MASER EMISSION

In this section, we discuss the specific cases of the lines which present a potential maser effect, using the same LVG code of Section 3. Transitions with inverted level population (masing lines) are characterized by negative optical depths and negative excitation temperatures and the strongest masers have the largest negative optical depths. Fig. 7 shows the optical depth τ of the transition $3_{1,2}$–$2_{2,1}$ at 225.9 GHz. Negative values of τ are observed at 100 and 200 K, for column densities above 10^{14} cm^{-2}. The largest negative optical depth, $\tau = -1.1$, is reached for column densities between 2 and

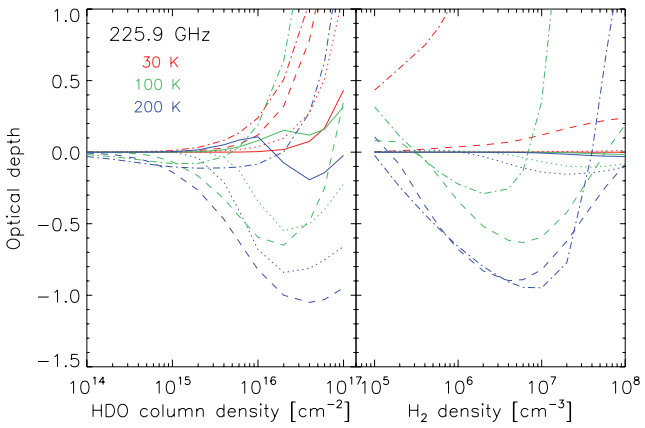

Figure 7. Optical depth τ of the transition $3_{1,2}$–$2_{2,1}$ at 225.9 GHz. Different colours refer to different temperatures: 30 K (red), 100 K (green) and 200 K (blue). In the left-hand panel, different lines refer to different H_2 densities: 10^5 cm^{-3} (solid lines), 10^6 cm^{-3} (dotted lines), 10^7 cm^{-3} (dashed lines) and 10^8 cm^{-3} (dash–dotted lines). In the right-hand panel, different lines refer to different HDO column densities: 10^{14} cm^{-2} (solid lines), 10^{15} cm^{-2} (dotted lines), 10^{16} cm^{-2} (dashed lines) and 10^{17} cm^{-2} (dash–dotted lines).

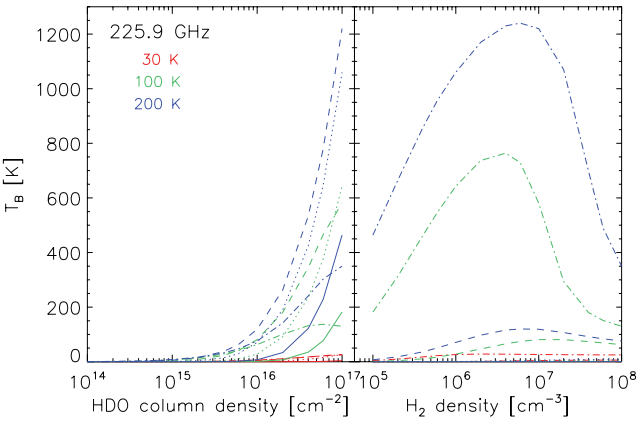

Figure 8. Brightness temperature $T_{\rm B}$ (in K) for the transition $3_{1,2}$–$2_{2,1}$ at 225.9 GHz. Lines and colours are as in Fig. 7.

8×10^{16} cm^{-2} and a H_2 density between 2 and 20×10^6 cm^{-3}. The corresponding brightness temperatures, $T_{\rm B}$, are plotted in Fig. 8. It is observed that $T_{\rm B}$ can reach 1200 K for a HDO column density of 10^{17} cm^{-2} and H_2 densities between 2 and 8×10^6 cm^{-3}.

Six other lines were found to invert in the frequency range 0–2000 GHz, notably the often observed 80.6- and 255.1-GHz lines. They are reported in Table 1. The inversions are found to occur for similar physical conditions: $T \sim 100$–200 K, N(HDO) $> 10^{15}$ cm^{-2} and $n(H_2) \sim 10^5$–10^7 cm^{-3}. The maximum brightness temperatures, $T_{\rm B} = 1200$ K, are observed for the two transitions at 80.6 and 225.9 GHz. We note that while the 225.9-GHz line also inverts with the excitation rate coefficients of Green (1989) (but at larger densities), the 80.6-GHz line, as well as the 5.7-GHz line, was not predicted to invert with the collisional coefficients of Green (1989). This is a particularly interesting result, as the 80.6-GHz line is observable and observed from ground telescopes. The masering effect, not previously identified, can help in explaining the observations obtained by Codella et al. (2010) towards the low-mass protostar L1448-mm. They found the 80.6-GHz emission associated with the hot corino of the source and a spot possibly associated with the outflow shock. Intriguingly, they noticed that the spatial position of this spot coincided with the distribution of the H_2O 22 GHz and, possibly, 183-GHz maser lines. The new collisional coefficients support the interpretation that the HDO observed emission is associated with regions of high densities, where the line mases.

As a final remark, we note that the conditions for the HDO lines to mase (relatively high densities, temperature and HDO column densities) can be found in several astronomical situations. First, in the hot cores and hot corinos of protostars, but also in the outflow shocks and the protoplanetary discs' innermost regions. Indeed, Ceccarelli et al. (2010b) noted that the 255.1-GHz line mases, by using the Green (1989) collisional coefficients, in protoplanetary discs.

5 CONCLUSIONS

We have reported rate coefficients for rotational transitions in HDO and D_2O induced by H_2 collisions below 300 K. Calculations were performed at the CC and CS levels with the deuterated variants of the H_2O–H_2 interaction potential of Valiron et al. (2008). The HDO–H_2 and D_2O–H_2 rate coefficients were compared to the corresponding rate coefficients for HDO–He (Green 1989) and H_2O–H_2

Table 1. HDO transitions presenting a population inversion. The ranges of column density, temperature and H_2 density where the optical depth τ is negative is given for each transition. The largest values of $|\tau|$ and T_B (brightness temperature) are also provided.

Frequency (GHz)	Transition	Density (cm^{-3})	Temperature (K)	N(HDO) (cm^{-2})	$\lvert\tau^{max}\rvert$	T_B^{max} (K)
0.8	$3_{3,0}$–$3_{3,1}$	5×10^5–10^8	100–200	$>2 \times 10^{16}$	3	60
5.7	$4_{3,1}$–$4_{3,2}$	2×10^6–10^8	100–200	$>10^{16}$	1	18
80.6	$1_{1,0}$–$1_{1,1}$	10^5–5×10^6	100–200	$>2 \times 10^{15}$	1	1200
120.8	$5_{1,5}$–$4_{2,2}$	10^5–10^8	100–200	$>2 \times 10^{15}$	2.5	550
138.5	$6_{1,6}$–$5_{2,3}$	10^6–10^8	100–200	$>2 \times 10^{16}$	2	150
225.9	$3_{1,2}$–$2_{2,1}$	10^5–10^8	100–200	$>10^{15}$	1	1200
255.1	$5_{2,3}$–$4_{3,2}$	10^6–10^8	100–200	$>10^{16}$	1.5	450

(Dubernet et al. 2006, 2009), respectively. Significant differences were observed and it was concluded (i) that the rate coefficients for H_2O provide only estimates for D_2O at the order-of-magnitude level and (ii) that He is not a good substitute for H_2 in the case of HDO, with differences up to three orders of magnitude. The impact of the new HDO rate coefficients was examined using non-LTE LVG modelling and it was shown that in the optically thin case the inaccuracies in excitation rate coefficients are quasi-linearly propagated within the radiative transfer equations. The present rate coefficients should therefore lead to a significant re-estimation of the HDO abundance and, therefore, of the D/H ratio of interstellar water (see e.g. Coutens et al., in preparation). A number of potential maser transitions were also identified in the frequency range 0–300 GHz, with optical depths larger than 1 in absolute value and brightness temperatures up to 1200 K. A particularly interesting result is the prediction of a masering effect in the 80.6-GHz line, supporting the interpretation that the HDO observed emission towards the low-mass protostar L1448-mm is associated with regions of high densities (Codella et al. 2010).

Finally, we note that in contrast to H/D isotopic substitution, isotopic effects for the oxygen isotopologues of water ($H_2^{17}O$ and $H_2^{18}O$) can be safely ignored since the change in internal geometries is essentially negligible and the C_{2v} symmetry is conserved.

ACKNOWLEDGMENTS

This work has been supported by the CNRS national programme 'Physique et Chimie du Milieu Interstellaire' (PCMI). Scattering calculations were performed on the CIMENT supercomputing platform in Grenoble with valuable help from F. Roch.

REFERENCES

Belpassi L., Reca M. L., Tarantelli F., Roncaratti L. F., Pirani F., Cappelletti D., Faure A., Scribano Y., 2010, J. Am. Chemical Soc., 132, 13046
Bergin E. A. et al., 2010, A&A, 521, L20
Butner H. M., Charnley S. B., Ceccarelli C., Rodgers S. D., Pardo J. R., Parise B., Cernicharo J., Davis G. R., 2007, ApJ, 659, L137
Ceccarelli C., Maret S., Tielens A. G. G. M., Castets A., Caux E., 2003, A&A, 410, 587
Ceccarelli C., Caselli P., Herbst E., Tielens A. G. G. M., Caux E., 2007, in Reipurth B., Jewitt D., Keil K., eds, Protostars and Planets V, Extreme Deuteration and Hot Corinos. Univ. Arizona Press, Tucson, p. 47
Ceccarelli C. et al., 2010a, A&A, 521, L22
Ceccarelli C., Cernicharo J., Ménard F., Pinte C., 2010b, ApJ, 725, L135
Codella C., Ceccarelli C., Nisini B., Bachiller R., Cernicharo J., Gueth F., Fuente A., Lefloch B., 2010, A&A, 522, L1
Comito C. et al., 2010, A&A, 521, L38
Coutens A. et al., 2011, A&A, submitted
Dubernet M.-L. et al., 2006, A&A, 460, 323
Dubernet M.-L., Daniel F., Grosjean A., Lin C. Y., 2009, A&A, 497, 911
Faure A., Gorfinkiel J. D., Tennyson J., 2004, MNRAS, 347, 323
Faure A., Valiron P., Wernli M., Wiesenfeld L., Rist C., Noga J., Tennyson J., 2005, J. Chemical Phys., 122, 221102
Faure A., Crimier N., Ceccarelli C., Valiron P., Wiesenfeld L., Dubernet M. L., 2007, A&A, 472, 1029
Green S., 1989, ApJS, 70, 813
Hartogh P. et al., 2011, Nat, 478, 218
Palma A., Green S., Defrees D. J., McLean A. D., 1988, J. Chemical Phys., 89, 1401
Phillips T. R., Maluendes S., Green S., 1995, J. Chemical Phys., 102, 6024
Schöier F. L., van der Tak F. F. S., van Dishoeck E. F., Black J. H., 2005, A&A, 432, 369
Scribano Y., Faure A., Wiesenfeld L., 2010, J. Chemical Phys., 133, 231105
Troscompt N., Faure A., Maret S., Ceccarelli C., Hily-Blant P., Wiesenfeld L., 2009, A&A, 506, 1243
Turner B. E., Fourikis N., Morris M., Palmer P., Zuckerman B., 1975, ApJ, 198, L125
Valiron P., Wernli M., Faure A., Wiesenfeld L., Rist C., Kedžuch S., Noga J., 2008, J. Chemical Phys., 129, 134306
van der Avoird A., Nesbitt D. J., 2011, J. Chemical Phys., 134, 044314
van der Avoird A., Scribano Y., Faure A., Weida M. J., Fair J. R., Nesbitt D. J., 2011, Chemical Phys., in press
Vastel C. et al., 2010, A&A, 521, L31
Wang X.-G., Carrington T., 2011, J. Chemical Phys., 134, 044313
Wiesenfeld L., Faure A., 2010, Phys. Rev. A, 82, 040702
Wiesenfeld L., Scribano Y., Faure A., 2011, Phys. Chemistry Chemical Phys., 13, 8230
Yang B., Stancil P. C., 2007, J. Chemical Phys., 126, 154306
Yang C.-H. et al., 2010, J. Chemical Phys., 133, 131103
Yang C.-H., Sarma G., Parker D. H., Ter Meulen J. J., Wiesenfeld L., 2011, J. Chemical Phys., 134, 204308

This paper has been typeset from a TEX/LATEX file prepared by the author.